# Growth and properties of strained $VO_x$ thin films with controlled stoichiometry

A. D. Rata<sup>1</sup>, A. R. Chezan<sup>2</sup>, and T. Hibma<sup>1</sup>

<sup>1</sup>Chemical Physics, Materials Science Centre, Rijksuniversiteit Groningen,
Nijenborgh 4, Groningen 9747 AG, The Netherlands and

<sup>2</sup>Nuclear Solid State Physics, Materials Science Centre, Rijksuniversiteit Groningen,
Nijenborgh 4, Groningen 9747 AG, The Netherlands

M. W. Haverkort, and L. H. Tjeng
II. Physikalisches Insitut, Universität zu Köln, Zülpicher Str. 77, 50937 Köln, Germany

H. H. Hsieh, H. -J. Lin and C. T. Chen Synchrotron Radiation Research Center, Hsinchu 30077, Taiwan (Dated: February 7, 2020)

We report on the growth of high quality epitaxial films of  $VO_x$  on MgO(001) substrates. The oxygen content as a function of oxygen flux was determined using  $O_2$  - RBS and the vanadium valence using XAS. The upper and lower stoichiometry limit found are similar to the ones known for bulk material (0.8 < x < 1.3). From the RHEED oscillation period a large number of vacancies for both vanadium and oxygen were deduced, i.e.  $\approx 16\%$  for stoichiometric VO. These numbers are very similar to those for bulk material having the same composition and consequently quite strain-insensitive. Based on this finding, we propose that the large vacancy concentrations found in monoxides of  $VO_x$ ,  $TiO_x$  and  $NbO_x$  are stabilized by ligand field splittings at low symmetry transition metal sites next to the vacancies. The electrical conductivity of the films is much lower than the conductivity of bulk samples having the same composition. This is attributed to an increase in the pseudo-gap at the Fermi level due to a decrease in the direct overlap between  $t_{2g}$  orbitals of neighboring metal ions in the coherently strained layers. The temperature dependence of the conductivity is consistent with a variable range hopping mechanism.

#### I. INTRODUCTION

Vanadium oxides have been intensively studied, especially V<sub>2</sub>O<sub>3</sub> and VO<sub>2</sub>, which show a metal-insulator transition as a function of temperature or doping and interesting magnetic properties<sup>1</sup>. These transitions are believed to arise from the change in strong electronic correlation mechanisms associated with crystallographic distortions<sup>1</sup>. The monoxide of vanadium  $VO_x(x = 0.8 -$ 1.3), on the other hand, got much less attention. Among the monoxides of the first transition metal series, only  $TiO_x$  and  $VO_x$  have itinerant d electrons. This is due to the direct overlap between the partly filled metal  $t_{2a}$ orbitals<sup>2</sup>. Another characteristic property of these oxides is the large number of both cation and anion vacancies, even for  $x = 1 (15\%)^3$ . The origin of the stability of such a high number of vacancies is according to Goodenough<sup>4</sup> due to a balance between a loss in Madelung energy and an increased overlap of the metal  $t_{2g}$  orbitals. Two electrons are trapped at each isolated anion vacancy, two holes at each isolated cation vacancy, thereby minimizing the associated loss in Madelung energy. Stoichiometric VO always remains disordered, whereas ordering of the vacancies was only reported for x between 1.2 and  $1.3^5$ .

A systematic investigation of the physical properties of  $VO_x$  and  $TiO_x$  has been carried out by Banus et al.<sup>3</sup>. Both compounds crystalize in the rocksalt structure. Despite their structural similarities, the electric and magnetic properties of these monoxides are quite different.  $TiO_x$  is a metallic paramagnet over the whole homogene-

ity range, while for  $\mathrm{VO}_x$  a transition from a metallic to a semiconducting type of behavior is observed at x close to 1. The susceptibility of  $\mathrm{TiO}_x$  is nearly temperature independent, while the magnetic susceptibility of  $\mathrm{VO}_x$  can be described by a Curie-Weiss law, which suggests that 3d electrons partially localize in  $\mathrm{VO}_x^6$ . Transport measurements show that the conduction electrons in  $\mathrm{VO}_x$  are not simple band electrons. Nekel et al. have calculated the band structure of stoichiometric VO and TiO. If a simple band picture would be valid, both materials should be metallic and have similar properties, which is not the case

Mott<sup>8</sup> and Goodenough<sup>4</sup> have given explanations in terms of vacancies and electron correlation effects. One important difference between these two systems is that the  $t_{2g}$  band is half-filled for  $V^{2+}$ , but not for  $Ti^{2+}$ . Mott<sup>8</sup> explained the conduction observed in polycrystalline  $VO_x$  in terms of overlapping Hubbard bands, a minimum or "pseudo-gap" occurring in the density of states. At the same time, Anderson localization is believed to occur in the overlap region due to the random field produced by vacancies. Goodenough<sup>4</sup> proposes a model where atomic vacancies stabilize the occupied states in the bottom half of the  $t_{2g}$  valence band. A pseudo-gap separates the  $t_{2g}$  band in two so-called bonding and antibonding half-bands.

The details of the electronic and magnetic structure, however, are still not clear. The main obstacle for a systematic study is the lack of pure and single crystalline material, with a well defined stoichiometry. Preparation is often found to be difficult since  $VO_x$  easily oxidizes to  $V_2O_3$ . These problems can be avoided by growing epitaxial films of  $VO_x$  on appropriate substrates with a careful optimization of the evaporation conditions.

Only very little work on films of  $VO_x$  has been done up to know. Metal supported vanadium oxides were investigated by several authors in connection with catalytic properties. Kishi et al. have studied the growth and structure of thin V oxide layers on  $Cu(100)^{9,10}$  and Ni(110)<sup>11</sup> surface and have found the formation of a V<sub>2</sub>O<sub>3</sub>- like oxide phase after room temperature oxidation on  $Cu(100)^9$ . A growth of VO(111)-like structures was observed when vanadium layers were oxidized at 250°C on both  $Cu(100)^{10}$  and  $Ni(110)^{11}$  surfaces. The growth of  $VO_x$  islands on Rh(111) has been studied by X-ray photoelectron spectroscopy (XPS)<sup>12</sup>. Surnev et al. found a  $VO/VO_2$  - like phase at low coverage on Pd(111) using scanning tunnelling microscopy (STM)<sup>13,14</sup>.  $VO_x(111)$ epitaxial ultrathin films grown on a Pt(111) substrate by evaporating metallic vanadium in a controlled H<sub>2</sub>O background was studied by XPS and Auger electron spectroscopy (AES)<sup>15</sup>. Thin films of  $VO_x$  have also been grown on TiO<sub>2</sub> substrates, because of the enhanced catalytic activity shown by titania-supported vanadium oxides 16. Sambi et al. 17,18,19 studied locally ordered VO<sub>x</sub> films with a thickness up to 4 ML grown on  $TiO_2(110)$  by evaporating vanadium metal at room temperature and subsequent annealing in vacuum for a short period of time, in order to promote the uptake of oxygen from the substrate. From a structural point of view, local order of their films is supported by X-ray photoelectron diffraction (XPD). In the examples mentioned above, the vanadium oxidation state was established on the basis of the position and shape of the V  $2p_{3/2}$  photoemission line. However, the uncertainty of stoichiometry of vanadia films remains, since the binding energies (BE) of V  $2p_{3/2}$  for different oxidation states are very close, a comparison between data obtained in Refs.(9) and (17) showing some discrepancies. Moreover, a determination of the physical properties of  $VO_x$  thin films is missing in these

Recently we have succeeded in growing high quality epitaxial thin films of  $\mathrm{VO}_x$  on cleaved MgO(100) substrates<sup>20</sup>. In this paper we report a detailed experimental study on the growth, structure, spectroscopic characterization and stoichiometry determination of these films. Also resistivity measurements on MgO capped  $\mathrm{VO}_x$  layers, with different oxygen content, are presented.

### II. EXPERIMENTAL

The experiments were performed in a UHV-MBE system, with a base pressure below  $1 \times 10^{-10}$  mbar, equipped with reflection high-energy electron diffraction (RHEED), low-energy electron diffraction (LEED) and X-ray photoelectron spectroscopy (XPS) facilities.

Rutherford backscattering spectrometry (RBS) and Xray diffraction (XRD) were used to characterize the thin films grown in the MBE system ex-situ. MgO(100) was chosen as the substrate because it has the same cubic rocksalt structure as  $VO_x$ , with a mismatch of about 3%. MgO blocks were cleaved ex-situ and immediately introduced into the UHV chamber where the substrates were cleaned by annealing at  $650^{\circ}C$  for 2 hours in 1x10<sup>-6</sup> mbar oxygen to remove hydrocarbon contaminations. Clean and well-ordered surfaces, as determined by XPS, RHEED and LEED were obtained. Vanadium (V) (purity 99.99%) was evaporated using an electron-beam evaporator (Omicron EFM3). The deposition rate of V, measured by moving a quartz crystal at the position of the substrate, was set to 0.7 - 0.8 Å/min. The vanadium was simultaneously oxidized by a beam of  $^{18}O_2$  (99.99%). The oxygen was supplied through a leak valve into a small buffer volume<sup>21</sup> connected to the vacuum chamber through a 35 cm long and 1 cm wide stainless steel pipe, ending at a distance of 10 cm from the substrate. The pressure in the buffer volume was measured with a Baratron capacitance manometer. In the following, the buffer volume pressure, being a measure of the oxygen flux, will be given in millivolts (mV). The variation in buffer pressure during deposition was less than 1%. VO<sub>x</sub> films with different stoichiometries were grown by varying the <sup>18</sup>O<sub>2</sub> buffer volume pressure, while keeping the V flux constant. During evaporation the background pressure was  $2x10^{-8}$  mbar or lower. The V and  $^{18}O_2$  beams can be abruptly and simultaneously stopped. After closing the <sup>18</sup>O<sub>2</sub> valve the background pressure dropped to below  $10^{-9}$  mbar within seconds, insuring a well-defined oxygen exposure of the sample. All the samples were grown while keeping the substrate at room temperature (RT).

RHEED was used to monitor the evolution of the films. Thicknesses were calibrated by monitoring the RHEED intensity oscillations during deposition. We used the assumption that each oscillation corresponds to the formation of one new atomic monolayer (ML). Film thicknesses were also measured *ex-situ* with XRD.

XPS measurements were performed using non-monocromatic Al K $\alpha$  radiation ( $h\nu=1486.6$  eV) and the total energy resolution of the electron analyzer in combination with the photon source is about 1 eV.

To determine the oxygen content, RBS measurements have been performed. For calibration purposes a  $V_2O_3$  epitaxial thin film was also grown on an  $Al_2O_3(0001)$  substrate, with the oxygen partial pressure and the substrate temperature set at  $10^{-6}$  mbar and  $550^{\circ}\mathrm{C}$  respectively<sup>22,23,24</sup>. All the measurements were done in a so-called 'random' orientation with respect to the crystalline axes, using a He<sup>+</sup> beam with 1.5 MeV energy. The backscattering yields were detected at an angle of 165 degrees. To avoid ex-situ post-oxidation, a thin MgO cap layer was grown for protection by Mg deposition in  $^{18}O_2$  atmosphere of  $1x10^{-8}$  mbar at room temperature.

The XRD measurements were done using a Philips

MRD diffractometer, equipped with a hybrid mirror/monochromator for Cu  $K_{\alpha}$  radiation, a 4-circle goniometer and a programmable slit in front of the detector.

The X-ray absorption spectroscopy (XAS) measurements were performed at the 11A Dragon beam line at the Synchrotron Radiation Research Center Taiwan, using the total electron yield mode. The light has a degree of linear polarization of 98% and an energy resolution of 0.16 eV for photon energies between 500 and 550 eV.

Resistivity measurements were performed in a commercial Quantum design PPMS system. The electrical measurements were done in the constant voltage mode and the current was measured along the [100] direction of the films by two and four point geometry. Electrical contacts consisting of 10 nm of Cr metal were evaporated ex-situ on the MgO substrates prior to introduction into the MBE system, in order to measure the resistance of as-grown  $VO_x$  films.

# III. EXPERIMENTAL RESULTS

# A. Growth of $VO_x$ thin films

For a wide range of incident oxygen fluxes, epitaxial growth of  $VO_x$  thin films on MgO(100) substrates was concluded from in situ RHEED and LEED analysis. Our MBE system geometry allows for monitoring changes in surface structure during film growth by RHEED. This low angle electron diffraction technique is particularly suited to thin film growth as it is highly sensitive to surface morphology. A RHEED pattern of a clean MgO(100) surface and 20Å thick  $VO_x$  thin film deposited on MgO(100) is shown in Fig.1. The beam was incident along the [100] direction. The basic RHEED pattern did not change during growth, suggesting that the film continues to grow as a rocksalt phase on top of the underlying substrate. Sharp streaks and the presence of Kikuchi lines indicate that the surface is still smooth after deposition of 10 monolayers (ML) of  $VO_x$ .

In most cases oscillations in the intensity of the specularly reflected beam were observed during growth. These oscillations are characteristic for a *layer-by-layer* growth mode, each oscillation corresponds to the formation of one atomic layer. Note that RHEED oscillations were observed at room temperature, which is considered to be a very low temperature for an oxide system. In Fig.2 an example of these growth oscillations is shown.

In Fig.3 a sequence of RHEED patterns which were taken after deposition of about 50 monolayers of  $\mathrm{VO}_x$  using different oxygen fluxes is presented. The oxygen content x is indicated on each RHEED pattern. The corresponding oxygen flux used can be found in the caption of Fig.3. In paragraph III.B we will explain how the x values were determined using RBS spectrometry. Varying the oxygen buffer pressure between 12 and 20 mV (0.82 < x < 0.97) epitaxial growth is obtained and sharp streaks can still be observed after deposition of 50 ML

 ${
m VO}_x$ . The distance between  ${
m VO}_x$  streaks is the same as between the MgO streaks. This is consistent with a coherent growth as determined ex-situ by XRD, which will be discussed in section III. C. The rocksalt structure of  ${
m VO}_x$  thin films was also confirmed by LEED. The LEED pattern displays the same square symmetry and periodicity as a MgO(100) surface.

Between 22 and 30 mV (1.1 < x < 1.31), MgO RHEED streaks fade away quickly after starting the growth and 3D-transmission spots appear, suggesting considerable roughening of the surface. The absence of a LEED pattern for the x=1.28 and x=1.31 cases confirms that the surface morphology is becoming increasingly disordered. Nevertheless, the presence of RHEED oscillations shows that the growth is still layer-by-layer like.

For an oxygen buffer pressure of less than 12 mV (x < 0.8) powder rings and extra spots were observed in RHEED. Vanadium atoms were not completely oxidized in the later case as deduced from XPS core level intensities.

Attempts to make  $\mathrm{VO}_x$  films at higher substrate temperature were unsuccessful. The RHEED pattern quickly disappeared or was getting very diffuse from the beginning.

The V-2p and O-1s core lines measured for three different films i.e vanadium metal on MgO(100),  $VO_x$  on MgO(100) and  $V_2O_3$  on  $Al_2O_3(0001)$  are shown in Fig.4. The binding energies were corrected for the charging effect by assuming a constant binding energy of the O 1s peak at 531 eV. All spectra were corrected in a standard manner for the satellites due to the  $K\alpha_3\alpha_4$  components of the incident X-ray and an integral background was subtracted afterwards. The binding energies of the V  $2p_{3/2}$ peak found are given in the figure. The binding energy corresponding to the V  $2p_{3/2}$  in the VO<sub>x</sub> film was found between the ones corresponding to V metal and V<sub>2</sub>O<sub>3</sub>, respectively (see Fig.4). The vanadium oxidation state can be in principle determined from the position and shape of the V  $2p_{3/2}$  feature. Nevertheless, due to the fact that vanadium with different oxidation states has rather similar values for the binding energies $^{25}$  we did not perform a quantitative analysis of the XPS data. In order to determine precisely the stoichiometry we have adopted a different route, which will be presented in the following section.

#### B. Stoichiometry determination

The oxygen content of the films was determined from RBS measurements. As was mentioned already in the experimental part,  $^{18}O_2$  instead of  $^{16}O_2$  was employed for film growth to distinguish between the oxygen of the film and substrate. Using a 1.5 MeV He<sup>+</sup> beam, a good mass separation between  $^{16}$ O from the substrate and  $^{18}$ O from the film can be obtained. This can be observed in Fig.5 showing a RBS spectrum of a  $V_2O_3$  layer grown epitaxially on an  $Al_2O_3(0001)$  substrate, which was used

for calibration. A nice hexagonal LEED pattern characteristic for the corundum structure was observed, proving the high quality and long range order of the  $V_2O_3$  film. In Fig.6 part of the spectra for a capped and uncapped  $VO_x$  layer on MgO(001) is shown. In both spectra a well-separated <sup>18</sup>O-peak is visible. For the uncapped layer, an additional shoulder at the <sup>16</sup>O position can be observed due to the fact that the layer is post-oxidized in air. The absence of this shoulder in the spectrum of the capped layer proves that capped  $VO_x$  films are really protected from post-oxidation.

With the following formula we have calculated the ratio between the numbers of V and O atoms in a  $VO_x$  film, using  $V_2O_3$  as a reference sample.

$$x = \frac{3}{2} \frac{\left[\frac{A_O}{A_V}\right]_{VO_x}}{\left[\frac{A_O}{A_V}\right]_{VO_x}} \tag{1}$$

The areas  $A_O$  and  $A_V$  in the RBS spectra were determined by fitting the V and  $^{18}\text{O}$  peaks from  $\text{VO}_x$  and  $V_2O_3$  samples to a gaussian function, in the case of the  $^{18}\mathrm{O\text{-}peak}$  after subtraction of the linear background due to Mg. The <sup>18</sup>O-peak area was corrected for the contribution of the caplayer, using the thickness of the  $VO_x$ films and the Mg<sup>18</sup>O caplayer, as determined from the RHEED oscillations. The resulting x-values are plotted in Fig. 7 as a function of the oxygen buffer volume pressure for two series of samples. One can observe that the x values are nicely reproducible. The error in the determination is about 3\%. The upper and lower stoichiometry limit found are similar to the ones known for bulk material. For the sample grown at 10 mV the vanadium metal is not completely oxidized, as deduced from the XPS spectra. For x bigger than 1.3 a mixture of two phases was found.

# C. Structure of $VO_x$ thin films

From RHEED and LEED patterns it was already concluded that  $VO_x$  films grow epitaxially on MgO(100). To analyze the epitaxy and crystal structure of the films in a more quantitative way, we also performed an ex-situ XRD analysis. The measurements were done on samples capped whith a 18-20Å thin epitaxial MgO film.  $\theta$ - $2\theta$  scans show only weak diffraction peaks close to the (002) and (004) peaks of the MgO substrate, as expected from films having a rocksalt structure. The reflections are broadened due to the finite thickness of the film. There are no peaks corresponding to other phases. Moreover, for samples made with the oxygen buffer pressure varying between 12 and 22 mV a number of subsidiary thickness fringes were observed, suggesting a well defined composition and thickness of the film (see Fig.8).

To determine whether the growth is fully coherent or partially relaxed, the most convenient way is to measure the intensity profile around a non-specular reflection common to the substrate and the overlayer. This can be done by performing a set of  $2\theta$  -  $\omega$  scans at different  $\omega$ ,  $2\theta$ and  $\omega$  being the detector and sample orientations with respect to the beam direction. These scans can be easily mapped into reciprocal space. An example of such a map for the region in reciprocal space around the (113) reflection is shown in Fig.9. The horizontal and vertical axes are k vectors parallel  $(k_{par})$  and perpendicular  $(k_{per})$  to the surface plane, respectively. The intensity scale in the figure is logarithmic. The feature corresponding to the  $VO_x$  film can be clearly distinguished. The elongated shape of the MgO reflection perpendicular to the radial direction is due to mosaic spread. The peaks of MgO and  $VO_x$  are at the same  $k_{par}$  value, which proves that the film is fully coherent. Consequently,  $VO_x$  thin films experience a compressive strain in the perpendicular direction, which is induced by the lattice mismatch.

The lattice constant normal to the substrate surface can be determined from  $\theta$  -  $2\theta$  scans around MgO(002) or MgO(004) peaks using the Bragg law.  $2\theta$  values were determined by fitting the peaks to a gaussian function. The perpendicular lattice constant is plotted in Fig.10 as a function of the oxygen content. We found that the perpendicular lattice constant and consequently also the average lattice constant is decreasing with increasing oxygen content. This is in contrast to the behavior reported by Banus<sup>3</sup> for bulk VO<sub>x</sub>.

The layer thicknesses determined from X-ray specular reflectivity (XRR) measurements were in good agreement with the values obtained from the RHEED intensity oscillation period.

# D. Vacancy concentration

As was already mentioned in the Introduction, a large number of both vanadium and oxygen vacancy is characteristic for bulk  $\mathrm{VO}_x$ . Using a combination of RHEED and RBS resuls, an estimation of the number of vacancies present in  $\mathrm{VO}_x$  thin films can be made. RHEED oscillation periods were determined for all the  $\mathrm{VO}_x$  samples as well as for a calibration  $\mathrm{V_2O_3}$  thin film on  $\mathrm{Al_2O_3}$  (0001). All samples were grown using the same value for the vanadium flux. By comparing the time needed to grow one monolayer of  $\mathrm{VO}_x$  and  $\mathrm{V_2O_3}$  and assuming that  $\mathrm{V_2O_3}$  is stoichiometric and free of vacancies, the fraction of vacant vanadium sites  $(V_V)$  in  $\mathrm{VO}_x$  can be directly calculated. The oxygen vacancy concentration  $(V_O)$  can be obtained because x is already known from RBS, using the following expression:

$$x = \frac{1 - V_O}{1 - V_V} \tag{2}$$

As illustrated in Fig.11, the vanadium vacancy concentration is increasing with increasing oxygen content x, while the oxygen vacancy concentration is decreasing.

The total number of vacancies  $(V_V+V_O)$  is also decreasing with x. Close to the stoichiometric value we found about 16 % vacant sites of both vanadium and oxygen.

# E. Valence of the V ions from XAS

XAS measurements were done at the O K- edge in order to verify the valence of the V and O ions. The data are depicted in Fig.12 for samples with the oxygen content x (as determined from RBS) between 0.8 and 1.3. For comparison, we have also included the spectrum of a  $V_2O_3$  film in top part of the figure. The O K-edge absorption spectra correspond to the dipole-allowed transitions from the O 1s to the O 2p shell, which is partially empty due to the hybridization with V 3d conduction band states. The spectral structures that can be observed are dictated by these V 3d states  $^{27,28,29}$ .

The distinct peak observed at photon energies around 532 eV, can be assigned to transitions into the empty V 3d- $e_a^{\uparrow}$  band<sup>29</sup>. Structures at higher photon energies can be ascribed to transitions to the higher lying V 4sprelated bands. Important is to note that for the most oxygen deficient  $VO_x$  samples, i.e.  $x \ll 1$ , the lowest spectral structure is given by the 532 eV peak, indicating that the lower lying V 3d- $t_{2g}$  band is completely occupied by three electrons, and that thus the V valence is 2+ or less. For samples with higher oxygen content, i.e. for x > 1, a clear low energy peak appears at about 530 eV. This strongly suggests that holes are introduced in the V  $3d-t_{2q}$  band, meaning that the V valence is higher than 2+. This assignment is supported by the  $V_2O_3$  spectrum, in which transitions to both the  $t_{2q}^{\uparrow}$  and the  $e_q^{\uparrow}$ bands are possible because only two electrons occupy the three-fold degenerate  $t_{2q}^{\uparrow}$  orbital in this V<sup>3+</sup>  $3d^2$  system.

These XAS measurements show that the cross-over from less than 2+ to more than 2+ V valencies occurs for an RBS x value of about 0.94 - 0.97. This value is not very far from 1.00, and can be taken as an indication for a good agreement between the XAS and RBS methods.

We have also carried out XAS experiments at the V  $L_{23}(2p \to 3d)$  edges. The results are shown in Fig.13, in which we have also included the spectra for  $V_2O_3$  and  $Cr_2O_3$  for reference purposes. In going from x=0.8 to x=1.3 we can observe a gradual change in the spectra. Distinct and sharp structures start to develop for  $x \ge 1$ . The similarity of these structures with those of  $V_2O_3$  is striking, and in fact indicates that V ions in a 3+ valence state are present for  $x \ge 1$ , consistent with the observations at the O K edge mentioned above.

Important is the observation that the spectra are quite broad for x around 1. In the simplest approximation, one would expect to see a spectrum with the typical atomic multiplet structure of a  $2p^63d^3 \rightarrow 2p^53d^4$  transition of a  $V^{2+}$  ion in a  $O_H$  symmetry, as shown in the bottom curve of Fig.13. This curve has been calculated using standard parameters ( $10D_q \simeq 2 \text{ eV}$ ) often applied for the analysis of transition metal oxide soft-x-ray absorp-

tion spectra<sup>30,31</sup> and it shows quite distinct features with several peaks and valleys. Clearly, the experimental V  $L_{23}$  spectra for  $x \approx 1$  do not have these distinct features.

Also a comparison with the experimental spectrum of  $\operatorname{Cr_2O_3}$  (see Fig.13), which is also a  $3d^3$  ion in approximately  $O_H$  local symmetry, leads to the conclusion that the V  $L_{23}$  spectra are anomalously broad. We take this observation as an indication that the vanadium in VO is not all in the local  $3d^3-O_H$  symmetry, but that instead an appreciable amount of vanadium ions are experiencing strong local crystal fields of low symmetry associated with the presence of large amount of vacancies. These low symmetry crystal fields must be at least several hundreds of meV strong, in order to wash out completely the multiplet structure of a  $3d^3$ -ion in  $O_H$  symmetry. The implication of such crystal fields will be discussed in Section IV.

#### F. Transport properties

Electrical measurements have been performed to study the electronic structure of  $\mathrm{VO}_x$  films. Resistivity data have been reported previously by Banus³ for polycrystalline samples. Bulk material exhibits a semiconducting behavior for x>1, with an activation energy rising to about 40 meV for x=1.3. For x<1 VO $_x$  behaves like  $\mathrm{TiO}_x$ , with an almost temperature and composition independent resistivity of about  $3\mathrm{x}10^{-3}~\Omega\mathrm{cm}$ . Banus et al. reported a transition from a semimetallic to semiconducting type behavior in  $\mathrm{VO}_x$  at x=1.05.

The variation of logarithm of electrical resistivity of  $\mathrm{VO}_x$  thin films with different oxygen content is shown as a function of 1/T in Fig.14. The resistivity is increasing with decreasing T for all samples except the x=0.82 sample, suggesting a semiconductor-like behavior in the entire temperature range studied. However, it is evident in Fig.14 that  $\log \rho$  does not vary linearly with 1/T. Fig.15 shows the composition dependence of the activation energies calculated from the  $\log \rho$  - vs - 1/T plots close to room temperature. Note, that the apparent activation energy decreases with decreasing temperature.

Such behavior is similar to that described by Banus<sup>3</sup>. but we did observe a few important differences. Compared to the corresponding resistivity results for bulk samples we found a much higher absolute value of the resistivity. As can be observed from Fig.14 the transition from a metallic to a semiconductor type behavior is shifted from x = 1 (as found in bulk) to x = 0.8 for thin films. Moreover, the activation energy calculated close to room temperature (Fig.15) is larger. For example, for bulk stoichiometric VO, Banus et al.<sup>3</sup> obtained an apparent activation energy of only 5 meV. For thin films we found a much higher value of  $\approx 110$  meV. A slight increase in the activation energy can be observed going from x = 0.94 to x = 0.97. Although the oxygen content is changing only with 3\%, the activation energy is becoming almost two times larger. For  $x \approx 1.3$  the activation

energy rises to 180 meV.

The T-dependence of the resistivity is better described by variable range hopping behavior<sup>26</sup> given by:

$$\rho \approx \exp(\frac{T_0}{T})^{\frac{1}{4}} \tag{3}$$

This is evident from Fig.16 showing the normalized resistivity versus  $T^{-1/4}$ . This result is not surprising knowing that a high number of vacancies is characteristic for this material. A random field caused by vacant sites can produce localization of the electrons near the Fermi level just like in amorphous materials. Its occurrence in  $VO_x$  seems to be strong evidence that the vacancies play a major role, causing large changes in its electronic properties. The parameter  $T_0$  can be extracted from the slope of the curves in Fig.16.  $T_0$  is related to the density of localized states at the Fermi level  $N(E_F)^{32}$  by the following expression:

$$T_0 = \frac{24\alpha^3}{\pi N(E_F)k_B} \tag{4}$$

where  $\alpha^{-1}$  is the decay length of the wave function associated with the charge carriers and  $k_B$  is the Boltzmann constant. Taking a reasonable value for  $\alpha^{-1}$  as 5Å,  $N(E_F)$  can be calculated from the values of  $T_0$ . These parameters are tabulated in Table 1 together with the corresponding x values. Clearly, one can observe that for x=0.82 sample the density of localized states at the Fermi level is high and starts to decrease with increasing the oxygen content.

# IV. DISCUSSION

In general, it is difficult to determine the precise composition of ultra-thin films. However, in the previous section we have revealed that for oxidic systems accurate results can be obtained from RBS spectra, if  $^{18}\mathrm{O}_2$  is used for the growth of the film. On top of that, the layer-by-layer growth mechanism allowed us to determine the density of vacancies from the RHEED oscillation period.

It is interesting to compare the chemical and physical properties of these high-quality and well-characterized films with those of bulk material of the same composition. The main difference is that the films are coherent with the substrate and therefore highly strained. We found that this tensile stress does not affect the vacancy concentration significantly, but on the other hand induces strong changes in the transport properties. In the following we will discuss the consequences of these findings on our understanding of the electronic structure of vanadium monoxide and related compounds.

The presence of a large number of vacancies in  $VO_x$  and  $TiO_x$  remains one of the most puzzling characteristics of these compounds. The only other binary oxide

showing this behavior is NbO, which has about 25% vacancies in the rocksalt structure<sup>33</sup>. Apparently the creation of vacancies stabilizes the crystal by reducing the Gibbs free energy. According to Goodenough<sup>4</sup> the formation of vacancies leads to a reduction in the lattice constant, thereby broadening the  $t_{2g}$  bands. The resulting stabilization of the occupied valence band states is counteracted by a reduction in Madelung energy, but this energy loss is assumed to be minimized by a localization of the charge compensating electrons and holes near the oxygen and vanadium vacancies respectively. He argues that the application of hydrostatic pressure should reduce the vacancy concentration considerably and he refers to experiments giving indirect evidence in favor of this effect<sup>34</sup>.

The  $VO_x$  films we have grown epitaxially on MgO substrates are thin enough to be coherent with the substrate and are under tensile stress. In fact, the in-plane lattice constant is expanded (≈3%), while the out-of-plane lattice constant is reduced due to the Poisson effect. Applying Goodenough's arguments, much larger vacancy concentrations as compared to bulk material are expected, because on average the lattice is expanded considerably. In contrast to this prediction, however, we found that both the cation and anion concentration are not much affected. For stoichiometric VO the values are only slightly higher (of the order of 1 or 2%) than for bulk material, whereas for the extremal x values they are even significantly lower, in contrast to what is expected. Therefore, the stabilization of vacancies in  $VO_x$  is most likely due to a entirely different mechanism. Instead of being linked to the direct overlap between  $t_{2g}$  orbitals, it is conceivable that the stabilization is primarily related to the electrons and holes being trapped near the cation and anion vacancies in trap levels which are deep enough to cause an energy gain with respect to the defect free situation. According to Goodenough<sup>4</sup>, the  $t_{2q}$  orbitals of cations neighboring a cation vacancy are destabilized by a reduced bonding to neighboring  $t_{2q}$  orbitals and a stronger  $\pi$  bonding to the p orbitals next to the vacancy, thereby raising their energy above the Fermi level. On the other hand, near an oxygen vacancy the bonding  $t_{2q}$ orbitals are stabilized, whereas the  $e_g$  and s orbitals are less destabilized by the absence of oxygen  $p_{\sigma}$  orbitals at the vacant site. Although these effects may be important, we believe that a much more decisive factor is the stabilization by additional ligand field splittings due to a local symmetry lowering at transition metal sites next to the vacancies.

We will first discuss the case of oxygen vacancies. Neighboring divalent 3d metal ions are surrounded by five oxygen ligands in a square pyramidal arrangement with  $C_{4v}$  symmetry. The  $t_{2g}$  and  $e_g$  levels will be split into three non- and one doubly degenerate levels, the latter being the lowest, see Fig. 17. To compensate for the local charge loss, we assume that two electrons are trapped at or near the vacancy. One extreme possibility is that both electrons are trapped at the vacant site,

forming an F-center, the other is that the excess electrons are trapped at neighboring d-metal sites. Assuming that at least a fraction of the excess electrons is trapped at the d-metal ions, the average number of d electrons will be larger than two for Ti- and larger than three for Vions next to a vacancy. In both cases some ligand field stabilization energy is gained, owing to the electrons occupying the lower  $t_{2q}$  levels in  $TiO_{x<1}$  and the lower  $e_q$ level in  $VO_{x<1}$ . Similarly, two excess holes are assumed to be trapped near the d metal vacancies in  $TiO_{x>1}$  and  $VO_{x>1}$ . One extreme possibility is that the holes are residing at oxygen neighbors. Following a suggestion of Elfimov et al.<sup>35</sup>, this would give a stable configuration in which the holes are in a triplet state localized at the oxygen coordination polyhedron around the vacancy. However, in contrast to the case of CaO discussed by these authors, in a transition metal compound it is more likely that the two holes are located at next nearest neighbor transition metal ions. The presence of the cation vacancy leads to a local symmetry lowering  $(C_{2v})$  at these cation sites (Fig. 17). Also in this case a ligand field stabilization is anticipated, because the average number of d electrons on d-metal ions next to a vacancy will be less than two for Ti and less than three for V. In section III.E it was reported that the structure of the V  $L_{23}$  XAS spectra is smeared out considerably. We attribute this smearing to the various low symmetry ligand field splittings discussed above. To account for the observed broadening, the shifts must be of the order of several tenths of an eV, i.e. sufficiently large to warrant the stability of vacancies. Note that in this model the loss in Madelung energy is limited because the electrons and holes are trapped at or close to the vacancies. Obviously, the explanation given above in terms of low symmetry ligand field stabilization effects is rather speculative and needs confirmation by quantitative calculations of the energy of formation of the defect regions.

Although, as was argued above, the decrease of direct overlap between  $t_{2g}$  orbitals does not have a major effect on the stability of vacancies, it will change the band structure in the valence band region and consequently change the electrical properties in strained films. Expanding the lattice by epitaxial growth on a substrate with a larger lattice constant like MgO will decrease the bandwidth and therefore increase the gap. This explains the lower conductivity and higher room temperature activation energies found in our films. In the models proposed by Goodenough<sup>4</sup> and Mott<sup>8</sup>, the on-site Coulomb interaction U is assumed to open up a small energy gap

in the itinerant  $t_{2g}$  band. It is assumed that overlapping tails of localized states, which are related to the disorder associated with the large number of defects in the system, are present at the edges of these Hubbard bands. In this way Mott<sup>8</sup> explains why in bulk samples the conductivity vs temperature is semiconductor-like at high temperature, but is better described by a variable range hopping mechanism at low temperatures. The conductivity results for our films are consistent with this explanation. The main difference is that the resistivity and apparent activation energies of the films are much higher, and that the transition from semiconducting to metallic behavior is shifted to lower x values, i.e. from  $x \approx 1$  in bulk samples to  $x \approx 0.8$  in films.

### V. CONCLUSIONS

We have successfully grown epitaxial  $VO_x$  films on MgO(100) substrates. Up to at least 120Å the growth is coherent and layer-by-layer-like. <sup>18</sup>O<sub>2</sub> -RBS was introduced as a convenient method to determine accurately the stoichiometry of these ultrathin layers. Once the stoichiometry is known, the vacancy concentration of both vanadium and oxygen can be calculated from the time to grow one monolayer as determined from RHEED. The numbers turn out to be very similar to those for bulk material. This implies that it is very unlikely that the formation of a high concentration of vacancies is induced by the increased direct overlap between neighboring  $t_{2q}$  orbitals in a defective crystal as suggested by Goodenough<sup>4</sup>. Instead we suggest that the stabilization is due to additional ligand field splittings, as observed from XAS, at the low symmetry metal sites near the vacancies. However, the decrease in direct overlap between  $t_{2q}$  orbitals and the concomitant increase of the size of the pseudogap between the lower and upper  $t_{2q}$  Hubbard bands is held responsible for the much larger electrical resistivity in strained  $VO_x$  films.

# VI. ACKNOWLEDGEMENTS

We thank T. T. M. Palstra and D. O. Boerma for stimulating discussions, H. Bruinenberg and J. Baas for technical assistance. The research of M.W.H. and L.H.T. is supported by the Deutsche Forschungsgemeinschaft through SFB 608.

<sup>&</sup>lt;sup>1</sup> M.Imada, A.Fujimori, Y.Tokura, Rev. Mod. Phys. **70**, 1039 (1998).

P. A. Cox Transition Metal Oxides, Oxford University Pres, Oxford, (1995).

<sup>&</sup>lt;sup>3</sup> M.D.Banus, T.B.Reed, A.J.Strauss, Phys. Rev. B 5, 2775 (1972).

<sup>&</sup>lt;sup>4</sup> J.B.Goodenough, Phys. Rev. B **5**, 2764 (1972).

<sup>&</sup>lt;sup>5</sup> M.Morinaga, J.B. Cohen, Acta Cryst. A 35, 745 (1979).

<sup>&</sup>lt;sup>6</sup> N.Tsuda, K.Nasu, A.Fujimori, K.Siratori, Electronic Conduction in Oxides, Sringer-Verlag, 2000.

<sup>&</sup>lt;sup>7</sup> A. Neckel, P. Rastl, R. Eibler, P. Weinberger, K. Schwarz, J. Phys. C 9, 579 (1976).

- <sup>8</sup> N.F.Mott, Phyl. Mag. **24**, 935 (1971).
- <sup>9</sup> K.Kishi, K.Hirai, T.Yamamoto, Surf. Sci. **290**, 309 (1993).
- <sup>10</sup> K.Kishi, Y.Hayakawa, K.Fujiwara, Surf. Sci. **356**, 171 (1996).
- <sup>11</sup> K.Kishi, K.Fujiwara, J. Electron Spectrosc. Relat. Phenom. 85, 123 (1997).
- <sup>12</sup> T. Hartmann, H. Knozinger, Z.Phys.Chem. (Munich) **197**, 113 (1996).
- <sup>13</sup> F.P. Leisenberger, S.Surnev, L.Vitali, M.G.Ramsey, F.P.Netzer, J. Vac. Sci. Technol. A 17, 1743 (1999).
- <sup>14</sup> S.Surnev, L.Vitali, M.G.Ramsey, F.P.Netzer, Phys. Rev. B **61**, 13945 (2000).
- <sup>15</sup> M.Petukhov, G.A. Rizzi, G.Granozzi, Surf. Sci. **490**, 376 (2001).
- V.E.Henrich and P.A. Cox, The Surface Science of Metal Oxides (Cambridge University Press, Cambridge, 1994).
- <sup>17</sup> M.D.Negra, M.Sambi, G.Granozzi, Surf. Sci. **436**, 227 (1999).
- <sup>18</sup> M.D.Negra, M.Sambi, G.Granozzi, Surf. Sci. **461**, 118 (2000).
- <sup>19</sup> M.Sambi, M.D.Negra G.Granozzi , Thin Solid Films 400, 26 (2001).
- <sup>20</sup> A.D.Rata, S.Vongtragool, D.O.Boerma, T.Hibma, Thin Solid Films 400, 120 (2001).
- <sup>21</sup> F.C. Voogt, T.Fujii, M.A. James, T. Hibma, Phys. Rev. B 63,125409 (2001).
- <sup>22</sup> H.Schuler, S. Klimm, G. Weissmann, C. Renner, S. Horn, Thin Solid Films 299, 119 (1997).
- <sup>23</sup> H.Schuler, G. Weissmann, C. Renner, S. Six, S. Klimm, F. Simmet, S. Horn, Mat. Res. Soc. Symp.Proc., Vol 401, 61 (1996).
- <sup>24</sup> H. Schuler, S. Grigoriev, S. Horn, Mat. Res. Soc. Symp.Proc., Vol **474**, 291 (1997).
- <sup>25</sup> G. Sawatzky, D. Post, Phys. Rev. B **20**, 1546 (1979).
- <sup>26</sup> N. Mott, Metal-Insulator Transitions, Taylor&Francis (1990)
- M. Abbate, H. Pen, M.T. Czyzyk, F.M.F. de Groot, F.C. Fuggle, Y.J. Ma, C.T. Chen, F. Sette, A. Fujimori, Y.Ueda, and K. Kosuge, J. Electron spectros. Relat.Phenom. 62, 185 (1993).
- <sup>28</sup> F.M.F. de Groot, M. Grioni, F.C. Fuggle, J.Ghijsen, G.A. Sawatzky, H.Petersen, Phys. Rev. b 40, 5715 (1989).

- <sup>29</sup> J.van Elp, Arata Tanaka, Phys. Rev. B **60**, 5331 (1999).
- <sup>30</sup> See review by F.M.F. de Groot, J. Electron Spectrosc. Relat. Phenom. 67, 529 (1994).
- <sup>31</sup> See review in the Theo Thole Memorial Issue, J. Electron Spectrosc. Relat. Phenom. 86, 1 (1997)
- <sup>32</sup> A.R. Brown, C.P. Jarrett, D.M. de Leeuw, M. Matters, Synthetic Metals, 88, 37-55 (1997).
- <sup>33</sup> H. Erschbaumer, R. Podloucky, A. Neckel , J. Phys. F **15**, L279 (1985).
- <sup>34</sup> M.D. Banus, Mater. Res. Bull.**3**, 723 (1968).
- <sup>35</sup> I.S. Elfimov, S.Yunoki, and G. A. Sawatzky, Phys. Rev. Lett. **89** 89, 216403 (2002)

TABLE I: Parameters extracted from  $T^{-1/4}$  dependence of resistivity.

$x \text{ in VO}_x$	$T_0(K)$	$N(E_F)(cm^{-3}eV^{-1})$
		26
0.82	2.6	$2 \times 10^{26}$
0.84	$2 \times 10^{3}$	$2 \times 10^{23}$
0.89	$5\times10^4$	$8 \times 10^{21}$
0.94	$12 \times 10^{4}$	$3 \times 10^{21}$
0.97	$5 \times 10^{6}$	$1 \times 10^{20}$
1.1	$1 \times 10^{7}$	$4 \times 10^{19}$
1.28	$2 \times 10^{7}$	$2 \times 10^{19}$

FIG. 1: RHEED patterns recorded at an electron energy of 15 kV with the beam incident along [100] direction. (a) clean MgO(100) substrate.(b) 20Å VO $_x$ (100) thin film grown on MgO(100) substrate using 18 mV oxygen buffer pressure while keeping the substrate at room temperature.

FIG. 2: RHEED intensity oscillations of the specularly reflected electron beam observed during deposition of  $VO_x$  on MgO(100). The electron beam was incident along the [100] direction, with a primary energy of 15 kV.

- FIG. 3: Sequence of RHEED patterns observed after deposition of 50 ML VO $_x$  on MgO(100) at different oxygen fluxes while keeping the substrate at room temperature. The oxygen buffer pressure was varied between 10 mV and 30 mV: (a) 30 mV, (b) 27 mV, (c) 24 mV, (d) 22 mV, (e) 20 mV, (f) 18 mV, (g) 16 mV, (h) 14 mV, (i) 12 mV, (j) 10 mV. The electron beam was incident along [100] direction, with a primary energy of 15 kV.
- FIG. 4: V2p and O1s XPS spectra of (a)  $V_2O_3$  on  $Al_2O_3$  (0001), (b)VO<sub>x</sub> on MgO(001) and (c) vanadium metal on MgO(001)
- FIG. 5: RBS spectra of 1.5 MeV  $\mathrm{He^+}$  ions scattered from a  $\mathrm{V_2O_3}$  film epitaxial grown on an  $\mathrm{Al_2O_3}(0001)$  substrate. The  $^{18}\mathrm{O}$  peak can be clearly distinguished.
- FIG. 6: RBS spectra of 1.5 MeV He<sup>+</sup> ions scattered from  $VO_x$  film deposited on MgO(100). (a) with a thin (2nm) MgO caplayer, (b) without caplayer. An extra shoulder at the  $^{16}O$  position is observed due to postoxidation in the latter case.
- FIG. 7: The oxygen content x as a function of the buffer volume pressure as determined from RBS data for two series of  $VO_x$  samples.
- FIG. 8:  $\theta$ -2 $\theta$  X-ray diffraction measurement of 10nm thick VO<sub>x</sub> thin film prepared with x = 0.94. Only the (002) and (004) diffraction peaks characteristic of the rocksalt structure can be observed. The reflections from the film are broadened due to the finite thickness of the film. Subsidiary thickness fringes indicate a well defined composition and thickness of the film.
- FIG. 9: XRD map of reciprocal space around the non-specular (113) reflection of a 10nm thick VO<sub>x</sub> thin film with x = 0.94. The logarithm of the diffracted intensity as a function of the in-plane  $k_{\parallel}$  and out-of-plane  $k_{\perp}$  reciprocal lattice vectors is plotted. The x- and y- axis are in units of  $\frac{4\pi}{\lambda}$ , with  $\lambda = 0.15015$  nm.
- FIG. 10: Perpendicular lattice constant of  $\mathrm{VO}_x$  films with different oxygen content as a function of x as determined from XRD. The perpendicular lattice constant is decreasing with increasing x.
- FIG. 11: Vanadium and oxygen vacancy concentrations in  $\mathrm{VO}_x$  as determined from the period of RHEED oscillations. The number of vanadium vacancies is increasing with x, while the number of oxygen vacancies is decreasing.
- FIG. 12: O1s X-ray absorption spectra of  $VO_x$  samples with the oxygen content varying between 0.8 and 1.3.
- FIG. 13: V  $L_{23}$  X-ray absorption spectra of VO<sub>x</sub> samples with the oxygen content varying between 0.8 and 1.3.

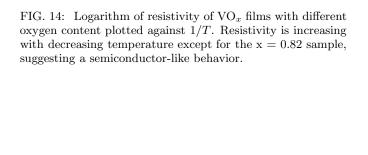


FIG. 15: Activation energy  $E_a$  versus x calculated for the temperature interval 150 < T < 300 K.

FIG. 16: Logarithm of normalized resistivity of  ${\rm VO}_x$  thin films with different oxygen content plotted as a function of  ${\rm T}^{-1/4}$ .

FIG. 17: Schematic ligand field splitting diagram for transition metal sites near an anion vacancy in a rocksalt structure having  $C_{4v}$  symmetry (right) and near a cation vacancy having  $C_{2v}$  symmetry (left).

